Flame Spread and Extinction over Thermally Thick PMMA in Low Oxygen Concentration Flow

Y. KUDO, M. ITAKURA, Y. FUJITA, and A. ITO
Faculty of Science and Technology
Hirosaki University
3 Bunkyo-cho
Hirosaki, 036-8561, Japan

ABSTRACT

This report discusses the mechanisms of flame spread and extinction over a thermally thick PMMA surface in a low-oxygen-concentration flow, based on experimental investigations. The temperature distribution in the condensed phase when the oxygen concentration in an air current decreases was measured in detail using holographic interferometry and thermography. The energy balance in the condensed phase was investigated based on the detailed temperature distribution, and the dominant heat transfer path in a low-oxygen-concentration flow was clarified. The net heat transfer rate in the direction normal to the surface, Q_y is little changed with a decrease in oxygen concentration, while the heat transfer rate in the direction parallel to the surface, Q_x decreases with oxygen concentration. The total heat transfer rate, Q_T also decreases, due to the decrease in Q_X. The radiative heat loss from unburned surface to surroundings, Q_R increases with decreasing oxygen concentration. The balance of heat in the unburned fuel falls drastically due to the increase in the ratio of radiative heat loss to the total heat transfer rate, Q_R/Q_T. This leads to flame extinction.

KEYWORDS: flame spread over solids, low oxygen concentration flow, flame extinction, holographic interferometry

INTRODUCTION

To understand the propagation and extinction mechanisms of a spreading flame along a combustible solid is important in predicting the behavior of the initial stage of building fires. The controlling mechanism of flame spread appears to differ with the surrounding conditions, such as the amount of ambient oxygen, gas flow velocity, direction of flame spread, and so on [1-4]. Recently, the influence of gravity in flame spread and extinction has also been investigated. It is reported that the extinction of a thermally thin solid fuel under microgravity conditions is significantly influenced by radiative heat loss from the unburned fuel surface [5]. The flame spread rate in air is controlled by the rate of thermal energy feedback from the flame to the unburned fuel surface [6,7]. Our latest thermally thick fuel experiments in opposed-airflow conditions [4] showed that the heat transfer rate from the gas phase is about 60% of the net total heat transfer rate in the non-opposed flow condition, while the heat transfer rate through the condensed-phase was over 80% near the extinction limit. Moreover, radiative heat loss was about 10% of the total heat transfer in flame spread over thermally thick solid fuel. When airflow velocity was increased, radiative heat loss was small enough not to have a major effect on extinction. From these results, it can be concluded that the extinction mechanism of a solid fuel changes depending on the surrounding conditions.

FIRE SAFETY SCIENCE–PROCEEDINGS OF THE EIGHTH INTERNATIONAL SYMPOSIUM, pp. 457-468

Most recently constructed buildings are quite airtight and have efficient insulation. When a fire occurs in such a highly airtight compartment, it would seem that the oxygen concentration in the involved compartment is decreased. However, few studies have been published dealing with flame spread over a solid fuel surface under low-oxygen-concentration conditions, and at present the details of the effect of oxygen concentration on flame spread over a solid fuel are not adequately understood [8]. In particular, the effect of the oxygen concentration on heat transfer from flame to unburned surface is unknown. Flame spread in microgravity conditions may be simulated by restricting the supply of oxygen with a low oxygen concentration, because flame spread in microgravity is controlled by the supply of oxygen.

In order to elucidate the heat transfer mechanism and determine the heat transfer path, we must know the detailed temperature structure both in the gas and condensed phases. Usually, thermocouples have been used for measuring temperature distributions [9-11]. However, with this technique it is difficult to determine the temperature gradient accurately due to limited spatial resolution. We recently used holographic interferometry (HI) combined with thermography to determine the temperature structure within a transparent material [3,4,12]. Careful use of these techniques can determine the heat flux distribution with high spatial resolution.

In this study, the detailed temperature distribution in a thick slab of polymethyl methacrylate (PMMA) during horizontal flame spread in low-oxygen-concentration opposed-flow conditions was measured. Based on the temperature structure in the condensed phase, the dominant heat transfer path and the extinction mechanism under low-oxygen conditions are discussed.

EXPERIMENTAL PROCEDURE AND APPARATUS

The wind tunnel used in this study, and details of the test section, are illustrated in Fig. 1. The wind tunnel is 400 mm long by 17 mm high and 34 mm wide, and is made of Pyrex. A rectification tube was installed ahead of the test section in order to provide uniform, laminar flow. The low-oxygen-concentration gas was made by mixing compressed dry air and nitrogen gas from a pressure tank, and supplied upstream from the rectification tube. The gas supplied to the wind tunnel was sampled upstream from the rectification tube using a gas-tight syringe. The oxygen concentration in the sampled gas was measured by gas chromatography. The opposed-flow rate was measured with a Pitot tube. By traversing the Pitot tube from top to bottom across the center of the wind tunnel, the velocity profile and the average velocity, $\bar{u}$, were obtained. Average airflow velocity in this experiment was fixed at 0.27 m/s (Reynolds number is about 470). We selected samples that were 10 mm wide, 25 mm thick, and 100 mm long. Pyrex plates 10 mm wide were installed on both sides of the PMMA sample with a small space between the sample and the Pyrex plate. This space is close to the quenching distance, about 2 mm, which prevents flames passing over both sides of the sample and ensures two-dimensional flame spread. These Pyrex plates affect the fringe shift only minimally because their thermo-optic coefficient and thermal expansion coefficient are much lower than those of PMMA.

The temperature distribution on the PMMA surface was recorded by thermography through an NaCl window in the top of the test section. The IR camera, with a 7.5-13 μm spectral range, has a temperature resolution of 0.1°C and a time resolution of 30 ms. The emissivity of the PMMA at 7.5-13 μm was determined to be 0.95 by calibrating the

temperature measured by thermography against that measured by a Chromel-Alumel thermocouple. Its emissivity is almost independent of its surface temperature, ranging from 0.90 to 0.99 below the glass transition temperature (about 105°C). The optical setup and the holographic procedure were described in Ref. [13].

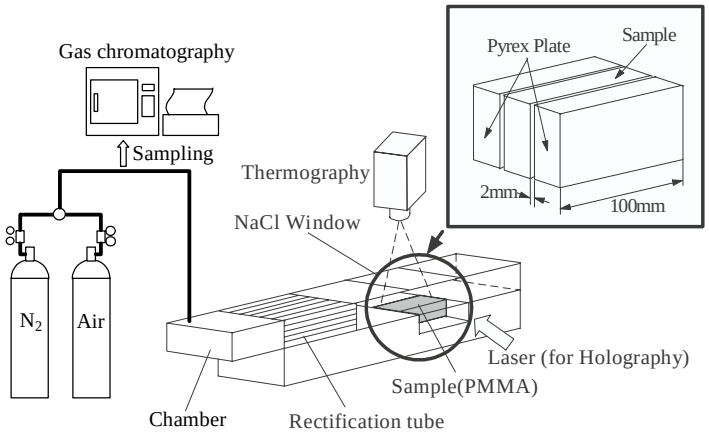

Fig. 1. Schematic illustration of the experimental apparatus.

The details of the HI measuring technique have been described previous papers [3,4,11], so only a brief description is presented here. The relationship between the temperature and the fringe number, *N*, can be expressed as

$$B\int_{T_\infty}^{T}(dn_p/dT)dT+\alpha B(T-T_\infty)\times[\int_{T_\alpha}^{T}(dn_p/dT)dT+n_{p\infty}-n_{a\infty}]=\lambda(2N-1)/2 \qquad (1)$$

where B is the width of the sample. The term dn_p/dT is the thermo-optic coefficient of the material; λ is the linear thermal expansion coefficient, n_p is the refractive index of the material at the ambient temperature, n_a is the refractive index of air at the ambient temperature, and k is the wavelength of the light. The thermo-optic coefficient and the linear thermal expansion coefficient of PMMA have been recorded up to a little over the glass transition temperature [12]. Above the glass transition temperature, accurate data for these coefficients are not currently available. Therefore, the surface temperature distribution measured by the IR camera was used as the reference temperature to analyze interference fringes above the glass transition temperature. For recording of holograms, the real-time method [14] was used. The optical setup and the holographic procedure were described in Ref. [13].

RESULTS AND DISCUSSION

Temperature Distribution in Condensed Phase

A schematic diagram of flame spread, including the coordinates, is shown in Fig. 2. The vaporization front on the sample surface is defined as $x = 0$ in this study, where x is a coordinate parallel to the sample surface. The sample surface is defined as $y = 0$, where y is the normal coordinate. The flame leading edge gradually retreats and the blue flame becomes small as the oxygen concentration decreases. With further reduction in the oxygen concentration, the flame retreated and extinguished. The oxygen concentration at

the extinction limit, $Y_{O2limit}$ was 18.4 vol.% in this test. Typical interferograms and isotherm contours within the condensed phase are shown in Fig. 3.

In these interferograms, it can be seen that part of the fringe pattern appears to be different from the rest. This is caused by the glass transition in the PMMA sample. The thermo-optic coefficient of PMMA decreases with increasing temperature (negative value), but the thermal expansion coefficient increases with increasing temperature [11]. Near the glass transition temperature, about 105°C, the term including these coefficients becomes zero. Therefore, the fringe pattern appears to be at a singular point at the glass transition temperature of PMMA. Except for this layer, the fringes shown in Fig. 2 correspond to isotherms.

The interval of the *x* direction of isotherm contours increases as oxygen concentration decreases. In other words, the interval of fringes increases in the *x*-direction. This means that the temperature gradient becomes small and the heat flux conducted to the unburned area through the condensed phase decreases. The interferogram photograph near the blow-off limit ($\bar{u}$ = 0.65 m/s) and isotherm contours are shown in Fig. 3e for comparison with those of oxygen concentration near the extinction limit (Fig. 3d). When airflow velocity is increased, the interval of the *x* direction of isotherm contours increases only slightly and it is suggested that the temperature gradient and the heat flux likewise barely increase. This is quite different than the effect of oxygen concentration.

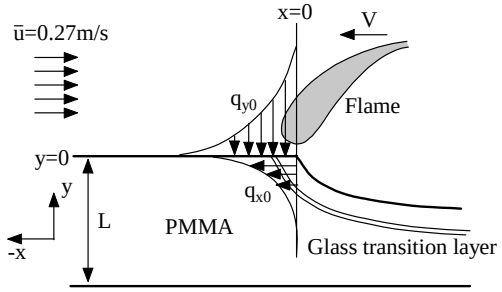

Fig. 2. Flame spread model.

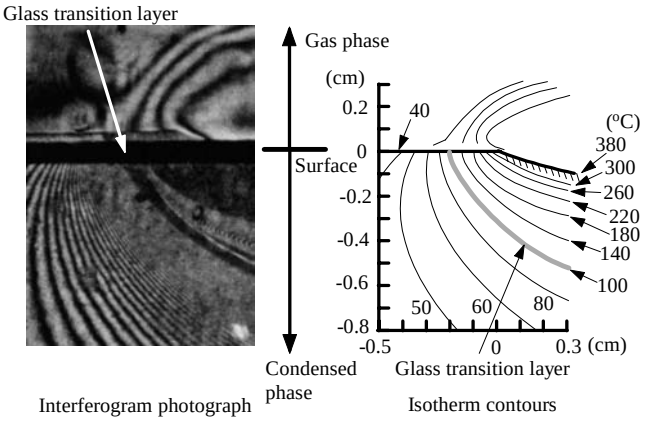

Fig. 3a. Typical interferogram photograph and isotherm contours at Y_{O2}=21.0 vol.% and $\bar{u}$=0.27 m/s case.

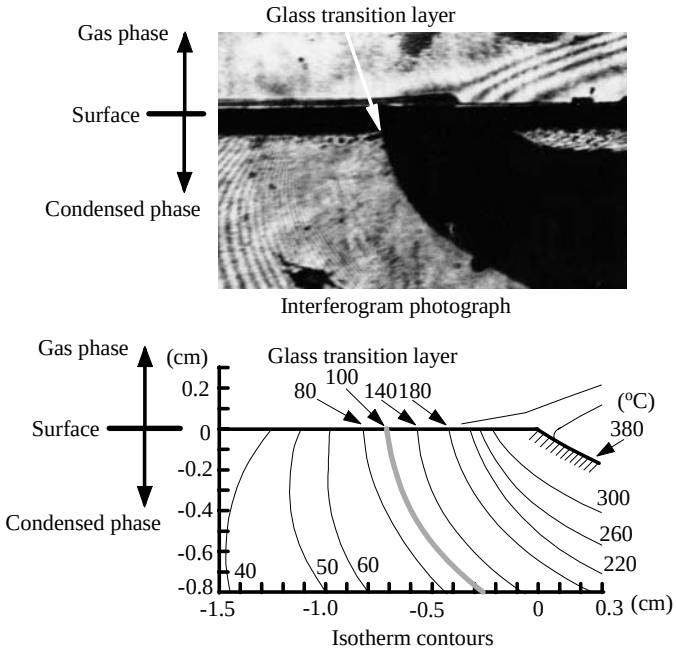

Fig. 3b. Typical interferogram photograph and isotherm contours at Y_{O2}=19.4 vol.% and $\bar{u}$=0.27 m/s case.

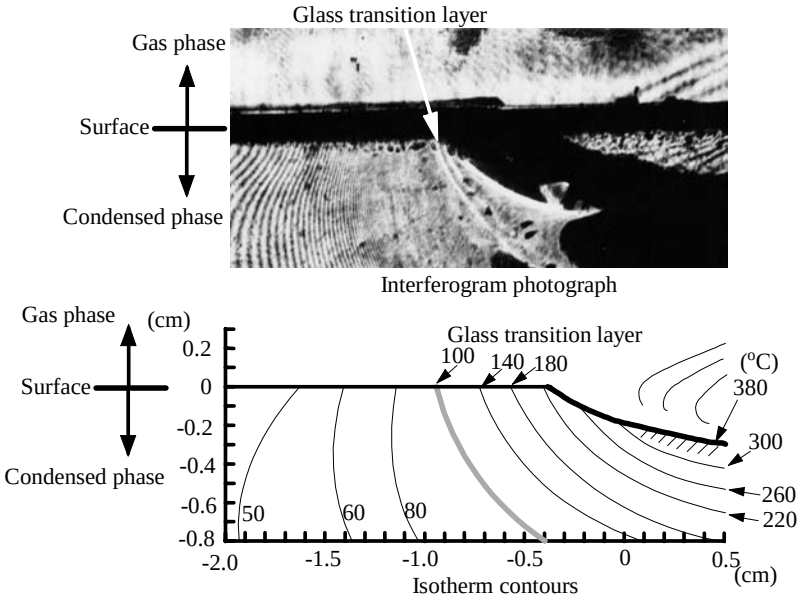

Fig. 3c. Typical interferogram photograph and isotherm contours at Y_{O2}=19.0 vol.% and $\bar{u}$=0.27 m/s case.

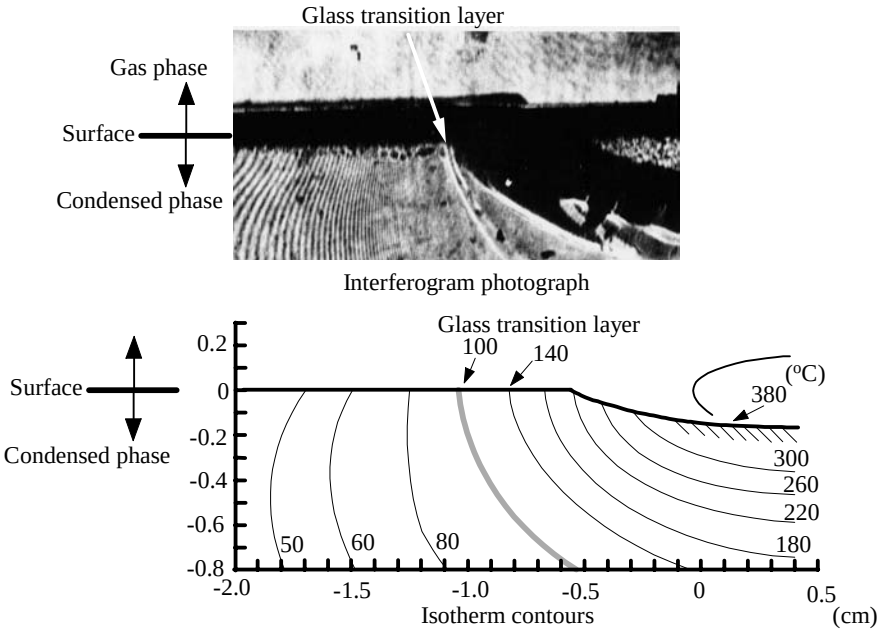

Fig. 3d. Typical interferogram photograph and isotherm contours at Y_{O2}=18.4 vol.% and $\bar{u}$=0.27m/s case (Extinction limit condition).

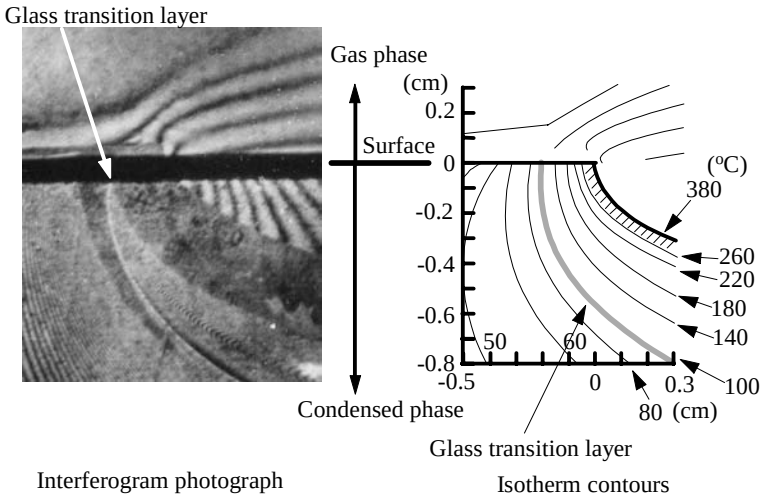

Fig. 3e. Typical interferogram photograph and isotherm contours at Y_{O2}=21.0 vol.% and $\bar{u}$=0.65 m/s case (Blow-off condition).

Surface temperature profiles across the sample width at its center, measured by thermography at various oxygen concentrations, are shown in Fig. 4. The surface temperature distribution in the preheat zone tends to increase with decreasing oxygen concentration. As the oxygen concentration decreases, the chemical reaction rate is

decreased and the flame temperature is decreased. The heat feedback from the flame to the unburned fuel is decreased, and the flame spread rate, *V*, is also decreased. Due to the decrease in *V*, the flame residence time required for heat feedback into the unburned fuel from the flame is increased. The increased residence time increases the heat conducted to the front of the unburned fuel. Therefore the preheating time becomes longer because the flame stays longer in front of the preheat zone due to the slow flame spread rate, and this causes the changed temperature distribution shown in Fig. 4.

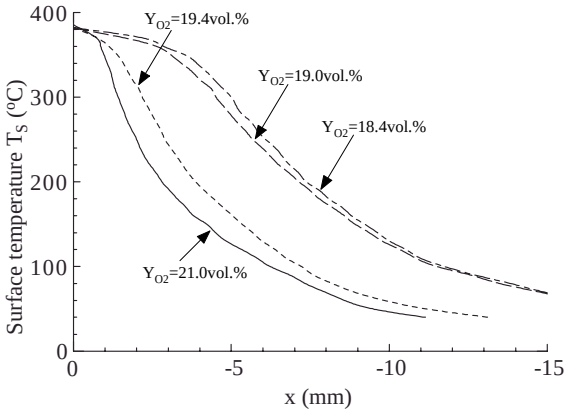

Fig. 4. Surface temperature distribution measured by thermography.

Heat Flux and Heat Transfer Rate

For quantitative evaluation of the heat feedback, the conductive heat flux in the direction normal to the surface at $y = 0$, q_{y0}, the conductive heat flux in the direction parallel to the surface at $x = 0$ (the vaporization front on the sample surface), q_{x0}, and radiative heat flux from surface to surroundings, q_r, are calculated based on the flame spread model shown in Fig. 2.

$$q_{y0} = \lambda_s \left.\frac{\partial T}{\partial y}\right|_{y=+0} = \lambda_g \left.\frac{\partial T}{\partial y}\right|_{y=-0} + q_{rf} - q_r \tag{2}$$

$$q_{x0} = \lambda_s \left.\frac{\partial T}{\partial x}\right|_{x=0} \tag{3}$$

$$q_r = \varepsilon_s \sigma (T_s^{\,4} - T_\infty^{\,4}) \tag{4}$$

where λ_s and λ_g are the thermal conductivities of the sample and gas, respectively. q_{rf} is the radiative heat flux from the flame to the unburned preheating surface, ε_s is the emissivity of the sample surface, and σ is the Stefan-Boltzmann constant. T_s is the surface temperature of the sample, and T_∞ is the ambient temperature. The first term on the right-hand side of Eq. 2 represents the convective/conductive heat flux from the gas

phase. The third term represents the radiative heat loss from the surface to surroundings. Therefore, q_{y0} is the net heat flux from the gas phase at the sample surface. By taking the spatial derivative of the temperature distributions, conductive heat flux in the direction normal to the surface, q_y, and the direction parallel to the surface, q_x, can be calculated. Since holographic interferometry has very high spatial resolution, the exact values of *dT/dx* and *dT/dy* were obtained, and they were compared with the values obtained from the temperature distribution measured using the thermocouple. The calculated values of q_{y0} are plotted in Fig. 5. The distribution of heat flux q_{y0} became smooth and the absolute value at the vaporization front, $x = 0$ also became small as the oxygen concentration was reduced. The net heat flux from the gas phase, q_{y0} at $x = 0$ in $Y_{O2} = 21.0$ vol.% was about 95 kW/m^2, becoming about 6 kW/m^2 in $Y_{O2limit} = 18.4$ vol.%, which is near the extinction limit. The heat conducted through the sample at the $x = 0$ plane, q_{x0} is plotted in Fig. 6. In the $Y_{O2} = 21$ vol.% case, q_{x0} increased rapidly near the surface. The values of q_{x0} on the surface were about 70 kW/m^2. The value of q_{x0} on the surface of the solid decreased as oxygen concentration decreased. The q_{x0} at $y = 0$ in oxygen concentrations near the extinction limit became about 5 kW/m^2. The radiative heat flux from the sample surface to the surroundings, q_r, which was calculated from the measured temperature distribution, is plotted in Fig. 7. It was found that the radiative heat flux far from the vaporization front was larger at lower oxygen concentrations.

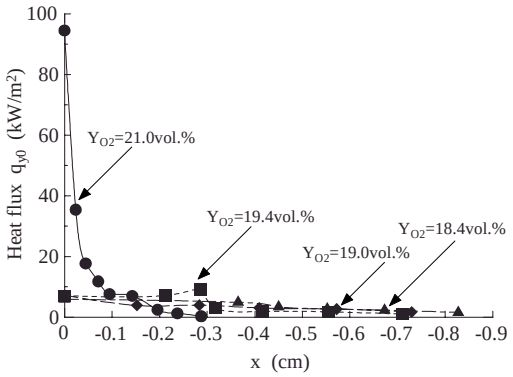

Fig. 5. Distribution of heat flux in the direction normal to the surface, q_{y0}.

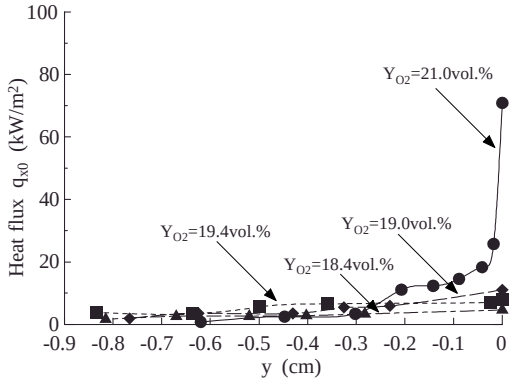

Fig. 6. Distribution of heat flux in the direction parallel to the surface, q_{x0}.

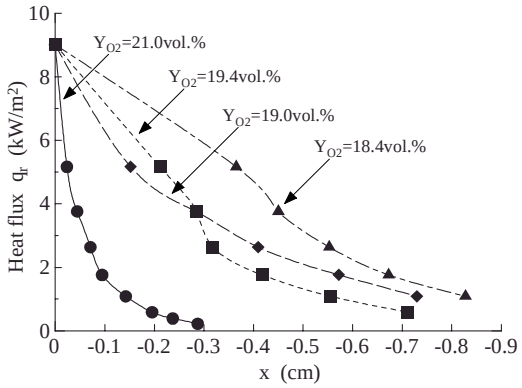

Fig. 7. Distribution of heat flux from surface to surroundings, q_r.

The energy balance in the condensed phase is constructed by using the temperature and heat flux distributions. The control volume is the layer from x = 0 to -∞ and y = 0 to -L (L is the depth of the sample). The total heat transfer rate into the control volume in the direction normal to the surface, Q_y, is

$$Q_y = \int_{-\infty}^{0} \lambda_s \left.\frac{\partial T}{\partial y}\right|_{y=0} dx = \int_{-\infty}^{0} q_{y0} dx \tag{5}$$

and the amount of heat transfer into the control volume through the plane x = 0 in the direction parallel to the surface, Q_x ,is

$$Q_x = \int_{-L}^{0} \lambda_s \left.\frac{\partial T}{\partial x}\right|_{x=0} dy = \int_{-L}^{0} q_{x0} dy. \tag{6}$$

The rate of heat loss from the rear sample surface is

$$Q_L = \int_{-\infty}^{0} \lambda_s \left.\frac{\partial T}{\partial y}\right|_{y=-L} dx. \tag{7}$$

Then, the total rate of heat transferred into the control volume is

$$Q_T = Q_y + Q_x - Q_L \tag{8}$$

Q_L is small in comparison with the other values, so it is assumed to be negligible. The rate of radiative heat loss from the control volume is

$$Q_R = \int_{-\infty}^{0} \varepsilon_s \sigma (T_s^{\,4} - T_\infty^{\,4}) dx. \tag{9}$$

The Q_R given in Eq. 9 is already included in the Q_y given in Eq. 5 because the given q_{y0} in Eq. 2 included the radiative heat loss from the surface to the surroundings. The following thermal properties were used to calculate the above integrals: thermal conductivity of the sample $k_s = 2.1 \times 10^{-1}$ W/m/K [14] and density $\rho_s = 1190$ kg/m^3 [16].

The calculated values of Q_y, Q_x, Q_T, and Q_R for each oxygen concentration are plotted in Fig. 8. When oxygen concentration decreases below $Y_{O2} = 21.0$ vol.%, Q_y is changed, while Q_x decreases near $Y_{O2} = 19.0$ vol.% concentration. Q_T also decreases due to the decrease in Q_X. On the other hand, Q_R increases with decreasing oxygen concentration. The relationship between the ratio Q_R/Q_T and oxygen concentration is shown in Fig. 9.

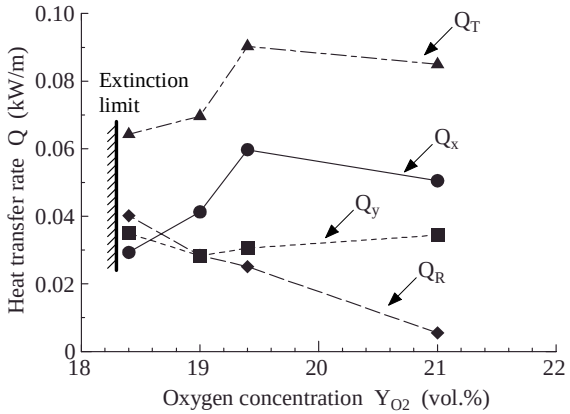

Fig. 8. Relationship between heat transfer rate and oxygen concentration.

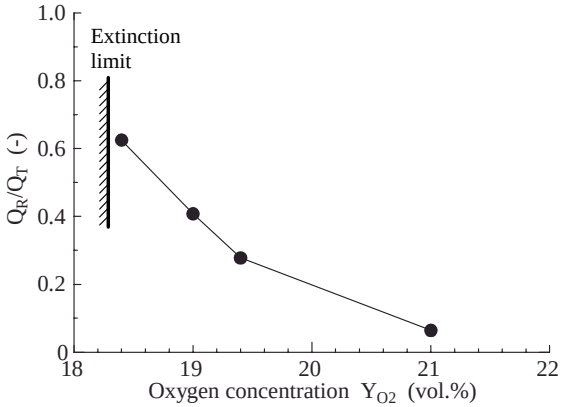

Fig. 9. Ratio Q_R/Q_T as a function of oxygen concentration.

In the case of $Y_{O2} = 21.0$vol.%, the radiative heat loss, Q_R was about 13% of the total heat transfer, Q_T. The ratio Q_R/Q_T increases as oxygen concentration is decreased. At $Y_{O2limit} =$ 18.4 vol.% oxygen (near the extinction limit), Q_R is about 60% of Q_T. At the low oxygen concentration near the extinction limit, it is difficult for the sample to receive sufficient heat feedback to maintain flame spread. The balance of heat at the sample surface falls

drastically due to the increased radiative heat loss, so eventually the flame must be extinguished.

CONCLUSIONS

The detailed temperature distribution near the flame leading edge during flame spread over PMMA in low-oxygen-concentration opposed-flow conditions was experimentally examined. Based on the temperature distribution, the energy balance in the condensed phase was investigated. The conclusions obtained from this study are summarized here.

1. The net heat transfer rate normal to the surface, Q_y, the net heat transfer rate parallel to the surface, Q_x, and the radiative heat loss from the surface, Q_R were obtained from measured isotherm contours and surface temperature profiles. The Q_y is little changing with decreasing oxygen concentration, while Q_x decreases near oxygen concentration, Y_{O2}=19.0 vol.%. The total heat transfer rate, Q_T also decreases due to the decrease in Q_x.
2. The radiative heat loss from surface to surroundings, Q_R increases with decreasing oxygen concentration because the surface temperature of the sample far from the flame front is higher at a lower oxygen concentration.
3. Near the extinction limit, there is barely enough heat feedback to the sample to support flame spread under low- oxygen-concentration conditions. The heat balance collapses as the ratio of radiative heat loss to the total heat transfer rate (Q_R/Q_T) increases, so eventually the flame must be extinguished.

REFERENCES

[1] Magee, R.S., and McAlevy III, R.F., "The Mechanism of Flame Spread," *J. Fire and Flammability*, **2**, pp. 271, (1971).

[2] Ray, S.R., and Glassmann, I., "The Detailed Processes involved in Flame Spread over Solid Fuels," *Combust. Sci. Technol*, 32:33-48 (1983).

[3] Ito, A. and Kashiwagi, T., "Characterization of Flame Spread over PMMA using Holographic Interferometry Sample Orientation Effects," *Combust. Flame*, **71**, pp. 189-204, (1988).

[4] Kudo, Y., and Ito, A., "Propagation and Extinction Mechanisms of Opposed-Flow Flame Spread over PMMA," *Proc. Combust. Inst.*, **29**, pp. 237-243, (2002).

[5] Takahashi, S., Kondou, M., Wakai, K., and Bhattacharjee, "Effect of Radiation Loss on Flame Spread over Thin PMMA Sheet in Microgravity," S., *Proc. Combust. Inst.*, **29**, pp. 2579-2586, (2002).

[6] Williams, F. A., "Mechanism of Fire Spread," *Proc. Combust. Inst.*, **16**, pp. 1281-1294, (1977).

[7] Fernandez-Pello, A.C., and Hirano, T., "Controlling Mechanisms of Flame Spread," *Combust. Sci. Technol.*, **32**, pp. 1-31, (1983).

[8] Ross, H.D., *Microgravity Combustion: Fire in Free Fall*, Academic Press, 2001, pp. 326-329.

[9] Fernandez-Pello, A.C. and Williams, F.A., "Laminar Flame Spread over PMMA Surfaces," *Proc. Combust. Inst.*, **15**, pp. 217-231, (1975).

[10] Hirano, T., Koshida, T., and Akita, K., "Flame Spread Mechanism over PMMA Surface," *Bull. Japan Assoc. Fire Sci. Eng*., **27**, pp. 33-39, (1977).

[11] Ray, S.R., Fernandez-Pello, A.C. and Glassmann, I., "A Study of the Heat Transfer Mechanisms in Horizontal Flame Propagation," *J. Heat Transfer, ASME*, **102**, pp. 357-363, (1980).

[12] Ito, A. and Kashiwagi, T., "Measurement Technique for Determining the Temperature Distribution in a Transparent Solid Using Holographic Interferometry," *Appl. Opt.*, 29:954-958, (1987).

[13] Ito, A., and Kashiwagi, T., "Temperature Measurements in PMMA during Downward Flame Spread in Air using Holographic Interferometry," *Proc. Combust. Inst.*, **21**, pp. 65-74, (1986).

[14] Vest, C.M., *Holographic Interferometry*, Willy, New York, 1979, Chapter 6.

[15] Hand, S.D. and Horsfall, F.J., "A Thermal Conductivity Apparatus for Solid and Molten Polymers," *J. Phy. E: Sci. Instrum.*, 8:687-690, (1975).

[16] Bares, V. and Wunderlich, B., "Heat Capacity of Molten Polymers," *J. Polym. Sci.*, 11:861-873, (1973).